Doppler-shifted cyclotron resonance of fast ions with circularly polarized shear Alfvén waves[a]

Yang Zhang,[1,b] W. W. Heidbrink,[1] Shu Zhou,[1] H. Boehmer,[1] R. McWilliams,[1] T. A. Carter,[2] S. Vincena,[2] and M. K. Lilley[3]

[1]*Department of Physics and Astronomy, University of California, Irvine, California 92697, USA*
[2]*Department of Physics and Astronomy, University of California, Los Angeles, California 90095, USA*
[3]*Department of Physics, Imperial College London, London, SW7 2AZ, United Kingdom*

The Doppler-shifted cyclotron resonance between fast ions and shear Alfvén waves (SAWs) has been experimentally investigated with a test-particle fast-ion (Li$^+$) beam launched in the helium plasma of the Large Plasma Device [Gekelman *et al.*, Rev. Sci. Instrum. **62**, 2875 (1991)]. Left- or right-hand circularly polarized SAWs are launched by an antenna with four current channels. A collimated fast-ion energy analyzer characterizes the resonance by measuring the nonclassical spreading of the averaged beam signal. Left-hand circularly polarized SAWs resonate with the fast ions but right-hand circularly polarized SAWs do not. The measured fast-ion profiles are compared with simulations by a Monte Carlo Lorentz code that uses the measured wave field data. © *2009 American Institute of Physics*. [DOI: 10.1063/1.3103813]

I. INTRODUCTION

Fast ions and Alfvén waves are pervasive in both natural[1,2] and laboratory plasmas.[3] The interaction of fast ions with Alfvén waves and instabilities is challenging to study experimentally because of difficulties in diagnosing the fast-ion distribution function and the wave fields accurately, in either fusion devices or space plasmas. In a hot fusion device, emitted particles are used to infer the distribution function in the core. In the solar-terrestrial plasma environments, where Alfvén waves constitute the dominant components of the EM wave spectra, expensive spacecraft measurements near the earth can cover but a fraction of the daunting space.

The fast-ion campaign at the Large Plasma Device (LAPD) (Ref. 4) at the University of California, Los Angeles has been focused on fast-ion transport and Alfvén activities in this linear device starting from the year 2002. So far, several experiments have been conducted in the device and reported, including a study of classical fast-ion transport,[5] the observation of a gap in the shear Alfvén wave (SAW) spectrum induced by an array of magnetic mirrors,[6] and a study of the Doppler-shifted resonance of fast ions with linearly polarized SAWs.[7] The unique LAPD provides a probe-accessible plasma that features dimensions comparable to magnetic fusion research devices, which can accommodate both large Alfvén wavelengths and fast-ion gyro-orbits.

The approach of the work reported here is to launch test-particle fast-ion beams with a narrow initial distribution function in phase space using plasma-immersible fast-ion sources.[8,9] Here the test-particle assumption is made since the energy transfer between the particles and waves is much smaller than the wave energy. The fast-ion beam is readily detected by a collimated fast-ion analyzer. When resonance overlap of fast ions and SAWs occurs, resonant beam transport in addition to the well calibrated classical transport[5] is analyzed with good phase-space resolution.

An earlier paper[7] described measurements in the LAPD of the Doppler-shifted cyclotron resonance of fast ions with SAWs. In that work, the waves were essentially linearly polarized and the main interaction region was only about one-third of the cyclotron orbit. The observed nonclassical spreading caused by the resonant interaction is in good qualitative and quantitative agreement with theoretical predictions. In particular, the maximum broadening occurs at the predicted wave frequency, and, as the frequency is varied, subsidiary peaks and nulls are observed at the expected locations. The work reported here extends this earlier study in several ways. With the exception of the SAW antenna, the hardware and experimental technique are identical to the previous work.

The organization of this paper is as follows: In Sec. II, the analytical theory for this work is summarized with the results from a Monte Carlo Lorentz code simulation. The experimental setup and fast ion and SAW diagnostics are introduced in Sec. III and the new experimental results are reported in Sec. IV. Conclusions are drawn in Sec. V along with planned future fast-ion transport studies.

II. RESONANCE THEORY AND SIMULATION

A. Resonance models

A charged particle is in cyclotron resonance with a transverse electromagnetic (EM) wave if the oscillation of wave electric field $\tilde{\mathbf{E}}$ matches the Doppler-shifted cyclotron motion of the particle.[10] In this case the following Doppler-shifted cyclotron resonance condition will be satisfied,

---

$$\omega - k_\parallel v_\parallel = \pm \, \Omega_f, \tag{1}$$

where ω is the wave frequency, $k_\parallel$ and $v_\parallel$ are the wave number and velocity components parallel to the equilibrium magnetic field $\mathbf{B}_0$, and $\Omega_f = q_f B_0 / m_f$ is the cyclotron frequency of the fast ions. The $\pm$ sign in Eq. (1) corresponds to the Doppler and anomalous Doppler resonances, where the resonant fast ions move slower or faster than the parallel wave phase speed $\omega/k_\parallel$, respectively. Equation (1) is however not a sufficient condition for effective energy exchange between waves and fast ions; the wave field itself is required to have the correct polarization. For example, ions gyrate in a left handed sense around magnetic field lines and so the most effective wave-particle interaction will occur for an EM wave satisfying Eq. (1) with an electric field that is circularly polarized in the same direction. In contrast with the previous work,[7] which investigated linearly polarized regions of the waves, this paper investigates the Doppler resonance of circularly polarized SAWs with fast ions. If not otherwise specified, the default polarization of the waves in this work is left handed.

Here the goodness of the resonance can be defined to be

$$(\omega - k_\parallel v_\parallel - \Omega_f)/\Omega_f \ll 1. \tag{2}$$

In the presence of an EM wave the fast ion motion is given by the Lorentz force law

$$\frac{d\mathbf{v}}{dt} = \frac{q_f}{m_f}(\widetilde{\mathbf{E}} + \mathbf{v} \times \mathbf{B}_0 + \mathbf{v} \times \widetilde{\mathbf{B}}),$$

$$\frac{d\mathbf{x}}{dt} = \mathbf{v}, \tag{3}$$

where $\widetilde{\mathbf{E}}$ and $\widetilde{\mathbf{B}}$ are the perturbed fields from the EM wave. In general, the rate of change of fast ion energy parallel and perpendicular to the background magnetic field can be represented as[11]

$$\frac{dW_\perp}{dt} = q_f \left\{ \widetilde{\mathbf{E}}_\perp \cdot \mathbf{v}_\perp + \frac{1}{\omega}[\mathbf{k}_\perp \cdot \mathbf{v}_\perp (\widetilde{E}_\parallel v_\parallel) - (k_\parallel v_\parallel)\widetilde{\mathbf{E}}_\perp \cdot \mathbf{v}_\perp] \right\},$$

$$\frac{dW_\parallel}{dt} = q_f \left\{ \widetilde{\mathbf{E}}_\parallel \cdot \mathbf{v}_\parallel - \frac{1}{\omega}[\mathbf{k}_\perp \cdot \mathbf{v}_\perp (\widetilde{E}_\parallel v_\parallel) - (k_\parallel v_\parallel)\widetilde{\mathbf{E}}_\perp \cdot \mathbf{v}_\perp] \right\}, \tag{4}$$

where the energy (W) change for each component is a combination of the work done by the wave electric field and a transfer of energy from the other component via the magnetic field. By following a gyrating fast ion's trajectory, a plane wave can be represented as a sum of helical waves moving coaxially with the fast ion as[11]

$$\mathbf{E} \sim \sum_{m=-\infty}^{\infty} J_m(\xi) \exp(ik_\parallel x_\parallel - i\omega t + im\phi), \tag{5}$$

where $\xi = k_\perp \rho_f$, ρ_f is the fast-ion Larmor radius, and ϕ is the gyroangle. By insisting that the fast ion must experience the wave at a constant phase in order to achieve effective wave-particle interaction, the resonance condition in Eq. (1) is obtained for $m = \pm 1$. For the $m = 1$ (the Doppler case) component of the wave, if the plasma is assumed to be sufficiently

cold to avoid finite Larmor radius effects, then the time averaged energy change for the fast ions in the wave field takes the approximate form[11]

$$\left\langle \frac{dW_\perp}{dt} \right\rangle = q_f \frac{\omega - k_\parallel v_\parallel}{\omega} v_\perp \widetilde{E}_+,$$

$$\left\langle \frac{dW_\parallel}{dt} \right\rangle = q_f \frac{k_\parallel v_\parallel}{\omega} v_\perp \widetilde{E}_+, \tag{6}$$

where $\widetilde{E}_+$ is the component of the perpendicular electric field that rotates in the same direction as the gyrating fast ions. From this it can be seen that unless a circularly polarized wave has the correct handedness, then no energy will be exchanged on average between the fast ions and the wave.

Efficient energy transfer can also occur via the parallel component of the wave electric field. For this the $m = 0$ part of the wave in Eq. (5) is required. The constant phase criterion then leads to the Landau resonance condition

$$\omega - k_\parallel v_\parallel = 0. \tag{7}$$

In this case the time averaged energy change for the fast ions becomes[11]

$$\left\langle \frac{dW_\perp}{dt} \right\rangle = 0,$$

$$\left\langle \frac{dW_\parallel}{dt} \right\rangle = q_f \frac{k_\parallel v_\parallel}{\omega} v_\parallel E_\parallel. \tag{8}$$

Experimentally, the most obvious change in beam-ion profile during interaction with the SAW is a change in gyroradius, suggesting that the energy change caused by the perpendicular electric field [Eq. (6)] dominates over the energy change caused by the parallel electric field [Eq. (8)]. As predicted by Eq. (6) [but not by Eq. (8)], significant energy exchange between the particles and the waves only occurs for left-handed polarization of the SAW (Sec. IV).

B. SAW dispersion relation

There are two regimes of plasma parameters for SAW propagation: the kinetic Alfvén wave (KAW) for plasma electrons having a Boltzmann distribution in the presence of the Alfvén wave fields and the inertial Alfvén wave (IAW) for electrons responding inertially to the wave. The KAW is more relevant to the physics of the interior regions of tokamak plasmas and the IAW to the edge and limiter regions. In this experiment, KAWs launched during the discharge of the LAPD are investigated.

A dimensionless parameter, $\bar{\beta}_e \equiv \bar{v}_{te}^2 / v_A^2$, is a quantitative measure of how inertial or kinetic a plasma is, where $\bar{v}_{\text{te}} = \sqrt{2T_e/m_e}$ is the thermal electron speed with T_e as the electron temperature. For example, if $\bar{\beta}_e \gg 1$, as in the discharge plasma of the LAPD, it is kinetic; if $\bar{\beta}_e \ll 1$, as in the afterglow plasma, the wave is inertial. For the KAW, the dispersion relation is

TABLE I. Comparison of time rates for different transport mechanisms.

Transport time scales	Time (ms)
Pitch angle scattering τ_{PAS}	5
Coulomb energy loss τ_W	1
SAW period τ_{SAW}	0.002–0.02
Cyclotron motion $\tau_{Cyclotron}$	~0.003

$$\omega^2/k_\parallel^2 = v_A^2(1 - \bar{\omega}^2 + k_\perp^2 \rho_s^2), \tag{9}$$

where $k_\parallel$ is the component of the wave vector parallel to the background magnetic field, $k_\perp$ is the perpendicular wave number, and ρ_s is the ion sound gyroradius [$\rho_s = c_s/\omega_{ci}$ with $c_s = (T_e/m_i)^{1/2}$]. In a typical case, $k_\perp^2 \rho_s^2$ is estimated to be 0.12. The intensity of the parallel wave electric field is[12]

$$\widetilde{\mathbf{E}}_\parallel = \frac{i\omega k_\perp \rho_s^2}{v_A(1 - \bar{\omega}^2)(1 - \bar{\omega}^2 + k_\perp^2 \rho_s^2)^{1/2}}\widetilde{\mathbf{E}}_\perp. \tag{10}$$

A typical ratio of $|\widetilde{\mathbf{E}}_\parallel/\widetilde{\mathbf{E}}_\perp|$ is 0.01, which means that the nonvanishing parallel electric field will slightly modify fast ion $v_\parallel$ in the resonance experiment. The perpendicular electric field can be calculated from Ampère's law and the dispersion relation,

$$\left|\frac{\widetilde{\mathbf{E}}_\perp}{\widetilde{\mathbf{B}}_\perp}\right| = \frac{v_A(1 - \bar{\omega}^2)}{(1 - \bar{\omega}^2 + k_\perp^2 \rho_s^2)^{1/2}}, \tag{11}$$

given measured wave magnetic field data (Sec. IV). To indicate the relative strength of different SAWs, B_{max} is defined in this article as the maximum amplitude of $\widetilde{B}_x$ in a specific z plane.

C. Monte Carlo simulation

A Monte Carlo Lorentz code[7,13] is used to simulate the SAW-induced fast-ion transport, with the classical transport caused by thermal ions and electrons included. In the LAPD discharge plasma, the electrons dominate Coulomb slowing down, while thermal ions dominate the pitch-angle scattering rate. A number of fast ions are launched numerically according to the initial beam divergence in phase space ($\pm 5°$ in pitch angle and ~ 5 eV in energy). Due to the difference in time scales of the transport mechanisms shown in Table I, the classical transport effects can be readily decoupled from the SAW influence in the code.

During the simulation of each fast-ion orbit, the pitch angle scattering event is considered at a randomly selected time ($t = t_1$), by which each gyroperiod is divided into two partitions ($\tau_{Cyclotron} = t_1 + t_2$). The single-particle Lorentz code is carried on throughout t_1 and t_2 for SAW perturbation. At the end of each time partition, the fast-ion energy is updated by the Coulomb slowing-down effect,

$$W' = W \exp\left(-\frac{t}{\tau_W}\right). \tag{12}$$

At $t = t_1$, a Monte Carlo collision operator[13] developed from the Coulomb scattering theory[14] is loaded to scatter the direction of the fast-ion velocity without changing its magnitude,[15]

$$\lambda_n = \lambda_0(1 - \nu_d\Delta t) \pm [(1 + \lambda_0^2)\nu_d\Delta t]^{1/2}, \tag{13}$$

where $\lambda = v_\parallel/v$, ν_d is the deflection collision frequency, and Δt is the time between each collisional event. After the desired number of gyroperiods, the fast-ion velocity and coordinates are recorded in the computer memory and the next fast ion is launched. SAW field data used in the Monte Carlo code comes from the measurements of b-dot probes (Sec. III)
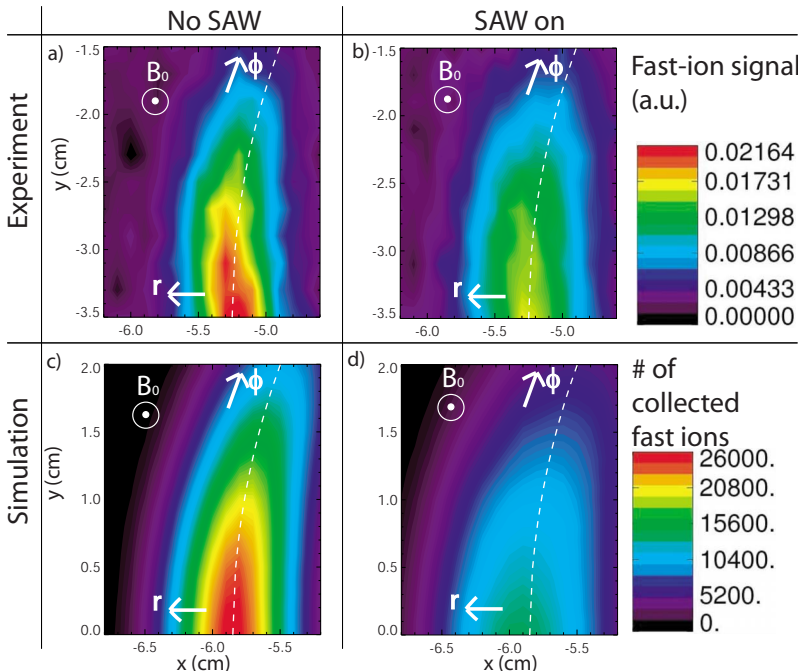
FIG. 1. (Color online) Comparison of Monte Carlo model simulated fast-ion beam profiles with experimental data. Contours in the same row use same color bar on the right for scaling. (Experimental orbit center is NOT LAPD center.)
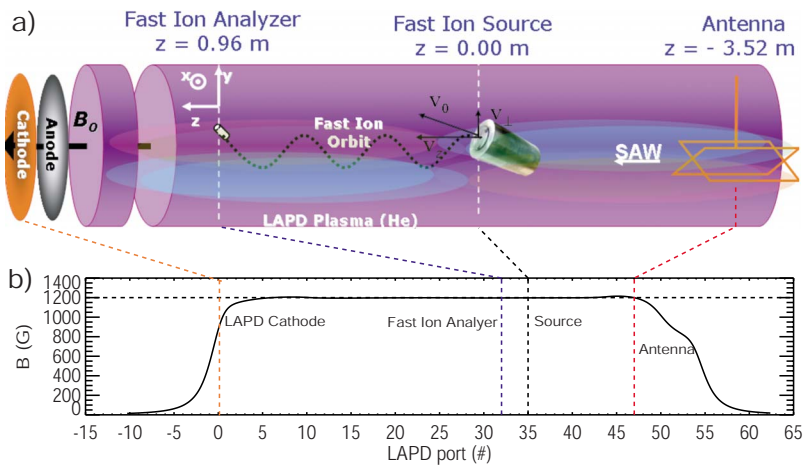
FIG. 2. (Color online) Experimental setup at the LAPD. (a) Overview of instruments (not to scale, dotted helix is the fast ion orbit; white box denotes the fast ion-SAW interaction region). (b) Ambient magnetic field profile vs LAPD port number (black solid). The distance between two adjacent ports is 0.32 m. Instruments' typical locations are marked by dashed perpendicular lines.

at the intermediate port between fast-ion source and detector. One million fast ion orbits are launched with random phases (φ_0) to contribute to the simulated beam profile several gyrocycles away. The final position and velocity vectors for each fast ion are stored for further beam profile collection. The simulated beam spatial profile shows substantial widening when the Doppler resonance condition is met.[7]

To compare the simulation results with experimental data collected by the fast-ion detector (Sec. III), the computed beam signals are simulated with a Lorentz code that calculates the fast-ion orbits inside the detector. The internal geometric and electric configurations of the detector are included in the code. Electric field lines are modeled by the COMSOL software (COMSOL, Inc.). When a fast ion enters the detector, its orbit is calculated by the Lorentz force law with the dc electric and magnetic fields inside the detector (SAW influence is negligible here). The number of fast ions collected at each position in the x-y plane is proportional to the collected signal strength (Sec. III). The simulated fast-ion beam profile can then be plotted by scanning a spatial grid near the orbit, similar to the motion of the probe in the experiment.

Contour plots generated by simulation are compared with experimental beam profiles in Fig. 1. During this experiment, to efficiently utilize the fast-ion source life time,[7] only the upper half of the beam spot is collected as shown in Figs. 1(a) and 1(b). Using the same color scale, the contour plot shows obvious widening in both the gyroradial ($\hat{r}$) and gyrophase ($\hat{\phi}$) direction when the SAW satisfies the resonance condition. Similarly, the simulated profiles show the same physics in Figs. 1(c) and 1(d).

III. EXPERIMENTAL SETUP

A. Overview

This experiment is performed in the upgraded LAPD, which has a 17.56-m-long, 1-m-diameter cylindrical main vacuum chamber. Pulsed plasmas (70 cm diameter, $\sim$10 ms in duration, 1 Hz repetition rate, and $\pm$10% spatial uniformity) are created by a discharge between a barium oxide coated cathode and a gridded molybdenum anode.[16] The cathode and anode are separated by 50 cm and both located

at the south end of the machine. The working gas is helium at a partial pressure of $\sim$3$\times$10^{-5} Torr with less than 3% of impurities. Typical average plasma parameters for this experiment are $n_i \sim 2.5 \times 10^{12}$ cm^{-3}, $T_e \sim 6$ eV, and $T_i \sim 1.0 \pm 0.5$ eV. The fast-ion beam density (5.0×10^8 cm^{-3}) used in this experiment is typically three to four orders of magnitude smaller than the plasma density, which ensures the test-particle assumption.

SAWs have been studied extensively in the LAPD. The waves are launched with inserted disk or loop antennas that drive propagating waves. Because of the large physical size, the plasma can accommodate up to ten axial wavelengths and the transverse wave structure is not determined by the radial dimensions of the plasma. The waves are partially reflected at the anode. Estimates indicate that $\sim$10% of the measured wave amplitude may be associated with the reflected wave.[7]

The hardware configuration is illustrated in Fig. 2(a) for this experiment. The origin of the z axis is defined as the location of the lithium fast-ion source (Sec. III B). The beam-wave interaction region is $\sim$10 m downstream of the cathode to ensure radially uniform background plasma properties. The SAW antenna (Sec. III C) is located at $z=-3.52$ m to avoid the near field effect (typical SAW wavelength parallel to $\mathbf{B}_0$ is $\sim$4 m). The fast-ion analyzer (Sec. III B) scans fast-ion signals in the x-y plane 0.32–0.96

TABLE II. List of parameters for typical Doppler-shifted fast-ion resonance with SAWs.

Parameter	Value
$\mathbf{B}_0$ (kG)	1.2
W_0 (eV)	600
θ (deg)	49.3
ρ_f (cm)	5.9
Gyrocycle/port	1/1
n_e (10^{12} cm^{-3})	2.5
T_e (eV)	6
f_{ci} (kHz)	457 (He$^+$)
	261.5 (Li$^+$)
Resonance $\bar{\omega}$	0.65

$$I_2 = I_0 \, e^{(i\omega t \pm \pi / 2)}$$

$$I_1 = I_0 \, e^{(i\omega t)}$$
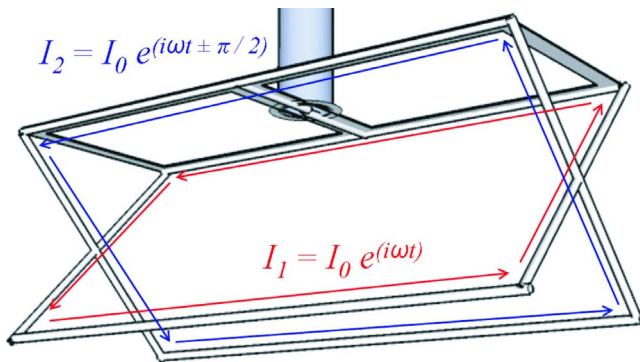
FIG. 3. (Color online) Illustration of the quadruple current channel antenna.

m away from the source to vary the interaction time between wave and particle. Figure 2(b) shows the actual LAPD port locations of all the instruments relative to the ambient magnetic field profile. The distance between two adjacent ports is 0.32 m. The axial magnetic field profiles are calculated from the actual current distribution for all the magnets in the machine.[17] The estimated axial field ripple amplitude at the radius of the machine is less than 2% for a constant field configuration.

In Table II, fast-ion orbit parameters, SAW frequency, and plasma conditions for the Doppler-shifted resonance studies in this work are listed.

B. Fast-ion sources and diagnostics

Lithium ion sources[8] with lithium aluminosilicate as thermionic emitters of different sizes (0.6 and 0.25 in. diameter, Heat Wave Inc.[18]) were designed, constructed, and characterized at the University of California, Irvine. For this transport study, the 0.6 in. emitter version with isotopically purified Li-7 [99.99% grade, experimentally determined to be greater than 90% (Ref. 19)] is operated with a 5 mm diameter circular aperture to achieve a narrow, high uniformity beam.

After the beam leaves the source and travels in the plasma and wave fields, a collimated fast-ion analyzer[7] is employed to produce a good fast-ion signal-to-noise in the strong rf noise environment during the LAPD discharge. The analyzer contains a 3.2-mm-diameter collector, an identical dummy for differential amplification, and three molybdenum grids for variable electrical barriers.[8] Measurements of the beam profile and wave field utilize a two-dimensional (2D) probe drive system (± 0.5 mm precision) and take advantage of the highly reproducible plasma of the LAPD. At each spatial location, multiple time traces are collected with ten plasma shots repeated. The probe tip is then moved to the next spatial position according to the preselected grid and the process is repeated.

For this transport study, fast-ion parameters are always selected to complete integer numbers of gyrocycles that coincide with the location of diagnostic ports since the slightly divergent beam is only refocused at integer numbers of gyro-orbits, as described by the "geometrical effect" in Ref. 5. The beam originates from the circular aperture, experiences classical cross-field diffusion, and passes the collection x-y plane with a pitch-angle θ close to the initial value.

C. SAW antennae and diagnostics

In order to generate circularly polarized SAWs with selectable handedness, this work uses a newly designed quadruple channel antenna (Fig. 3), which is equivalent to two identical rectangular loop antennae[20] as used in the previous work.[7] Each current loop is 30 cm along $\mathbf{B}_0$ and generates a linearly polarized wave field pattern near the center of the loop in the x-y plane. The wave propagates along $\mathbf{B}_0$ without significant changes in amplitude and pattern. The second current loop generates another linearly polarized wave field driven at $\pm \pi/2$ phase difference from the first one. The combined wave field becomes left- or right-hand circularly polarized as described in Eq. (5). The fast-ion orbit is aligned with the wave field to maximize the resonant interaction.

The wave magnetic field is measured by a set of identically designed b-dot probes featuring three orthogonal, differentially wound induction coil pairs, which are sensitive to the time derivative of the wave magnetic field.[21] Each coil pair is connected to a differential amplifier to select the mag-
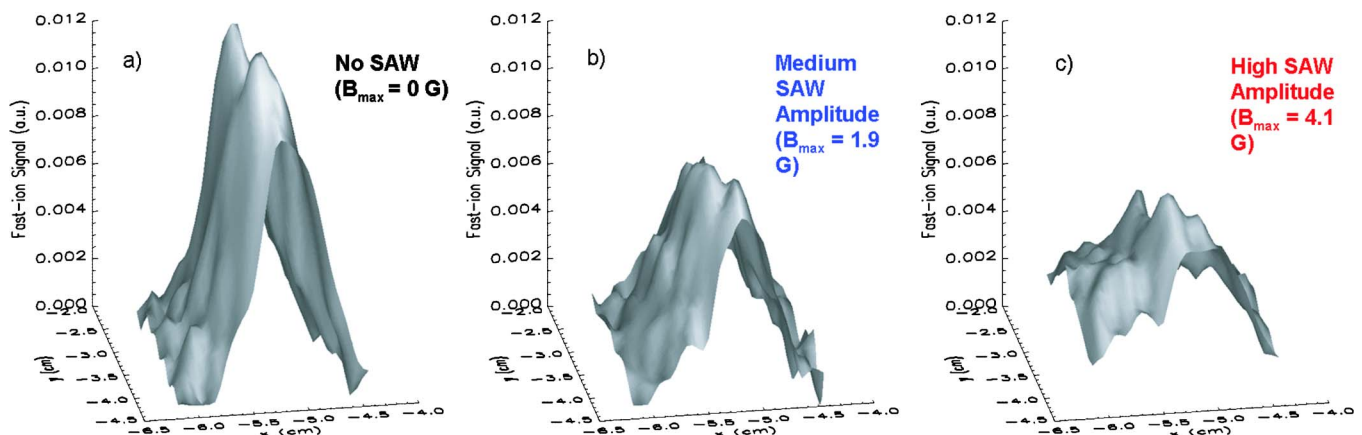
FIG. 4. (Color online) Comparison of fast-ion beam profile with different SAW amplitude. The z axis is fast-ion signal strength. (a) SAW antenna off. (b) Medium SAW amplitude ($B_{max} = 1.9$ G); c) High SAW amplitude ($B_{max} = 4.1$ G). (Data were acquired with 100 MHz sampling rate, averaging eight samples and ten consecutive plasma shots, August 2008 LAPD run.)
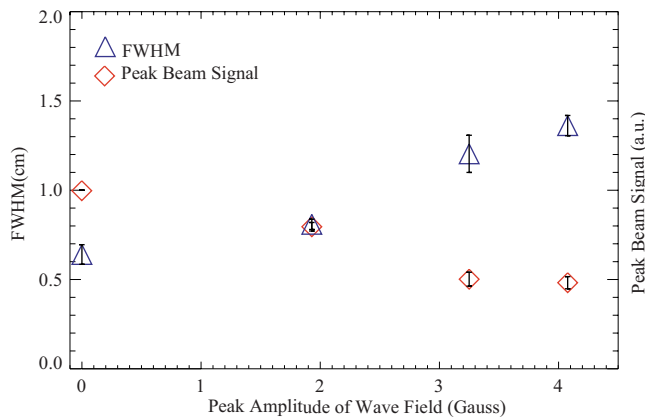
FIG. 5. (Color online) FWHM of the radial profile (triangle) and peak beam signal amplitude (diamond) vs wave amplitude B_{max}. The error bars are described from the standard deviation of the shots. The peak signal is normalized to the no-SAW case.

netic signal and reject common mode noise along each axis. Each probe is driven by the computer controlled motors to scan through the *x*-*y* planes along the region where fast-ion orbit covers in the LAPD.

D. System synchronization and data collection

Synchronization of the fast-ion source, the SAW antenna and the LAPD plasma is critical to a successful resonance experiment. It is arranged that the ∼20 ms fast-ion pulse is turned on and off every two plasma discharges, with an adjustable delay and duration to overlap in time with the ∼10 ms LAPD discharge. The background signal is taken when the source is disabled for one shot right after the previous beam-on shot. Even numbers of shots are repeated at one spatial location before the probe drive moves on. The signals with the source off are subtracted from the signals with the source on. The fast-ion signals shown in this work are net signals with the background subtracted.

Close to the end of each discharge, when the plasma parameters reach the best uniformity in time and space, the quadruple channel antenna drives an adjustable rf current for 1.0 ms, launching circularly polarized SAWs at the specified frequency. The data collection time window opens for

∼2 ms with ∼0.8 ms before the SAW duration. In this article, the SAW-influenced beam signal at each collection point (in the *x*-*y* plane) is averaged from 0.7 to 1 ms after the onset of the antenna current. The data before the SAWs are averaged to get the controls for no-wave situations. The time-averaged beam signals taken at a selected spatial grid are then combined to show the 2D fast-ion beam profile.

IV. FAST-ION RESONANCE RESULTS WITH CIRCULARLY POLARIZED SAWS

A. Fast-ion SAW induced transport is proportional to wave amplitude

The fast-ion beam profile shows significant widening as the SAW satisfies Doppler-shifted resonance condition (Fig. 1, experimental fast-ion orbits are different from machine center). The amplitude of the wave is adjusted at several different levels in order to observe the wave amplitude dependency. Here Fig. 4 shows the shade surfaces of the fast-ion beam signal profiles, where signal strength is the *z* axis. As the wave amplitude increases, the fast-ion profile becomes flatter and broader in both the $\hat{r}$ and $\hat{\phi}$ directions.

The changes in the full width at half maximum (FWHM) and the peak intensity are both good indicators[7] of the resonance effect and they are plotted against B_{max} in Fig. 5. The four sets of data points are acquired from the averaged fast-ion beam radial profiles at four different amplitudes of the waves. Linear dependence is not expected here since the resonance effect is an integration of the wave field influence along several gyrocycles and the experimental wave amplitude is not spatially uniform.

B. Selective fast-ion resonance with left-hand circularly polarized SAWs

The Doppler-shifted fast-ion resonance only happens when left-hand polarized SAWs are present to accelerate/ decelerate the fast-ion at the correct phases. The new quadruple channel antenna can select SAWs with different polarization directions relative to **B**$_0$. Resonance experiments are conducted with left- and right-hand polarized SAWs at the same frequency and amplitude. Here Fig. 6 compares the statistically averaged radial beam profiles for both polariza-
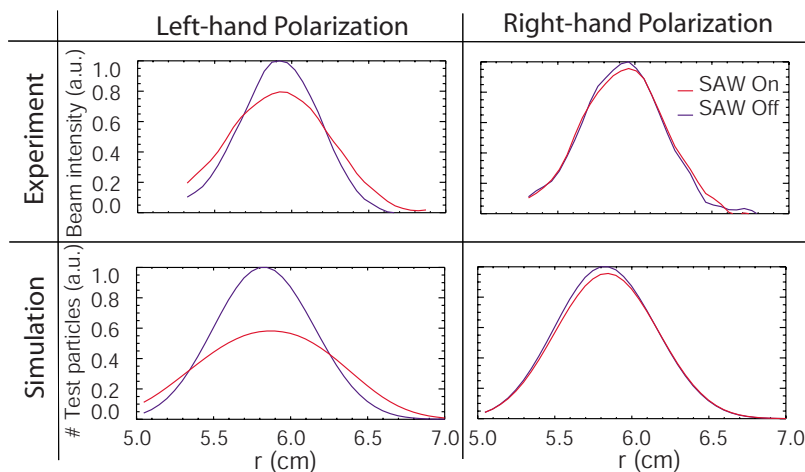
FIG. 6. (Color online) Comparison of fast-ion resonance effect with left-hand and right-hand polarizations.

tions with simulation results that use the measured wave field data. Both the experiment and the simulation show significant widening only for left-hand polarized waves. This confirms that the profile broadening is caused by changes in the fast-ion orbits rather than the field-line displacement produced by the SAW.

V. CONCLUSIONS AND FUTURE WORK

In this experimental work, the Doppler-shifted cyclotron resonance effect is directly measured from the beam spatial nonclassical spreading caused by circularly polarized SAWs. The resonance effect is observed to be dependent on the amplitude of the waves. Only the left-hand polarized SAWs resonate with the fast ions at the resonance condition.

Several extensions of this experimental study are possible. Simulation predicts that the fast-ion beam energy is changed up to ∼23 eV at the Doppler resonance condition with 1.6 G wave magnetic field amplitude. Direct measurements of energy changes could be obtained by biasing the fast-ion collector. A higher bandwidth fast-ion analyzer would permit detection of coherent oscillations in the collector current at the wave frequency. Observation over longer axial distances is also desirable.

More generally, the successful observation of fast-ion interaction with a single coherent Alfvén wave lays the groundwork for studies of more complicated wave-particle interactions, including interaction with Alfvén waves in the nonlinear regime and studies of fast-ion diffusion by drift-wave turbulence.

ACKNOWLEDGMENTS

[1] J. V. Hollweg and P. A. Isenberg, J. Geophys. Res. **107**, 1147, DOI:10.1029/2001JA000270 (2002).
[2] V. Shevchenko, V. Galinsky, and D. Winske, Geophys. Res. Lett. **33**, L23101, DOI:10.1029/2006GL026765 (2006).
[3] W. W. Heidbrink, Phys. Plasmas **15**, 055501 (2008) and references therein.
[4] W. Gekelman, H. Pfister, Z. Lucky, J. Bamber, D. Leneman, and J. Maggs, Rev. Sci. Instrum. **62**, 2875 (1991).
[5] L. Zhao, W. W. Heidbrink, H. Boehmer, and R. McWilliams, Phys. Plasmas **12**, 052108 (2005).
[6] Y. Zhang, W. W. Heidbrink, H. Boehmer, R. McWilliams, G. Chen, B. N. Breizman, S. Vincena, T. Carter, D. Leneman, W. Gekelman, P. Pribyl, and B. Brugman, Phys. Plasmas **15**, 012103 (2008).
[7] Y. Zhang, W. W. Heidbrink, H. Boehmer, R. McWilliams, S. Vincena, T. A. Carter, W. Gekelman, D. Leneman, and P. Pribyl, Phys. Plasmas **15**, 102112 (2008).
[8] Y. Zhang, H. Boehmer, W. W. Heidbrink, R. McWilliams, D. Leneman, and S. Vincena, Rev. Sci. Instrum. **78**, 013302 (2007).
[9] H. Boehmer, D. Edrich, W. W. Heidbrink, R. McWilliams, and L. Zhao, Rev. Sci. Instrum. **75**, 1013 (2004).
[10] T. H. Stix, *Waves in Plasmas* (American Institute of Physics, New York, 1992), pp. 238–246.
[11] A. V. Timofeev, in *Reviews of Plasma Physics*, edited by B. B. Kadomtzev (Consultant Bureau, New York, 1989), Vol. 14, p. 63.
[12] W. Gekelman, D. Leneman, J. Maggs, and S. Vincena, Phys. Plasmas **1**, 3775 (1994).
[13] L. Zhao, Ph.D. thesis, University of California, Irvine, 2005.
[14] A. H. Boozer, Phys. Plasmas **9**, 4389 (2002).
[15] A. H. Boozer and G. Kuo-Petravic, Phys. Fluids **24**, 851 (1981).
[16] D. Leneman, W. Gekelman, and J. Maggs, Rev. Sci. Instrum. **77**, 015108 (2006).
[17] S. Vincena, Ph.D. thesis, University of California, Los Angeles, 1999.
[18] Heat Wave Labs, Inc., 195 Aviation Way, Suite 100 Watsonville, CA 95076-2069, http://www.cathode.com/pdf/tb-118.pdf.
[19] Y. Zhang, Ph.D. thesis, University of California, Irvine, 2008.
[20] T. A. Carter, B. T. Brugman, and D. W. Auerbach, *Turbulence and Nonlinear Processes in Astrophysical Plasmas*, 6th Annual International Astrophysical Conference, edited by D. Shaikh and G. P. Zank (American Institute of Physics, New York, 2007).
[21] D. Leneman, W. Gekelman, and J. Maggs, Phys. Plasmas **7**, 3934 (2000).